Aluminosilicate weak colloidal gels: from the early age to the precipitation of zeolite

Electronic Supplementary Information (ESI†)

Arnaud Poulesquen[*a], Donatien Gomes Rodrigues[b], Bavand Keshavarz[c], Nicolas Courtois[a], Jan Ilavsky[d] and Gareth H. McKinley[e]

[a] *CEA, DES, ISEC, DPME, Univ Montpellier, F-30207 Bagnols-sur-Cèze, France CEA, DES, ISEC, DMRC, Univ Montpellier, F-30207 Bagnols-sur-Cèze, France*
[b] *CEA, DES, ISEC, DMRC, Univ Montpellier, F-30207 Bagnols-sur-Cèze, France*
[c] Department of Mechanical Engineering and Materials Science, Duke University, Durham, NC, USA
[d] *Advanced Photon Source, Argonne National Laboratory, Lemont, Illinois 60439, USA*
[e] *Hatsopoulos Microfluids Laboratory, Department of Mechanical Engineering, Massachusetts Institute of Technology, Cambridge, Massachusetts 02139, USA*

[*] *Corresponding author:*
arnaud.poulesquen@cea.fr

1   Experimental set-up for rheological measurements

Figures S1 and S2 present the method of preparation of the gel and the associated rheological protocol, that allows monitoring the evolution in the linear viscoelastic moduli during the gelation.
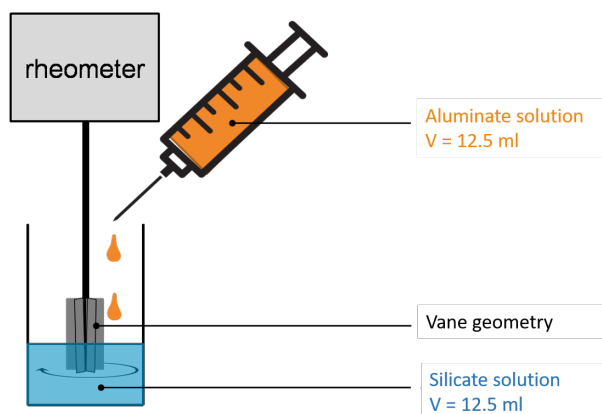

Fig. S1: Schematic representation of the *in situ* formulation of an aluminosilicate gel in the rheometer
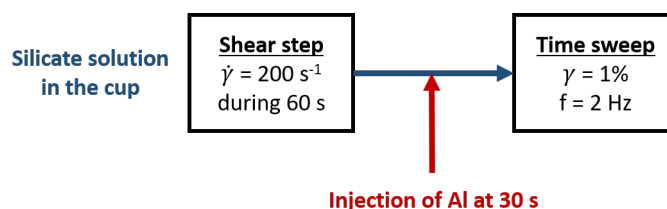

Fig. S2: Protocol for the time sweep experiments

2   Influence of the method of preparation of the gel

Figure S3 presents the influence of the addition of sodium hydroxide on the kinetics of gelation, when NaOH is introduced either in the silicate solution or in the aluminate solution. As discussed in the main text, the silicate species decondensate

and increase the hydroxide content, producing more reactive and mobile species in the system. When adding the silicate solution, the gelation is then faster, with respect to the addition of an excess of sodium hydroxide in the aluminate solution. However, the mechanical properties are very similar at the end of the gelation (e.g. compare the two [1.45 M] NaOH curves, meaning that it is the concentration of chemical species in the gel that drives its final mechanical properties.
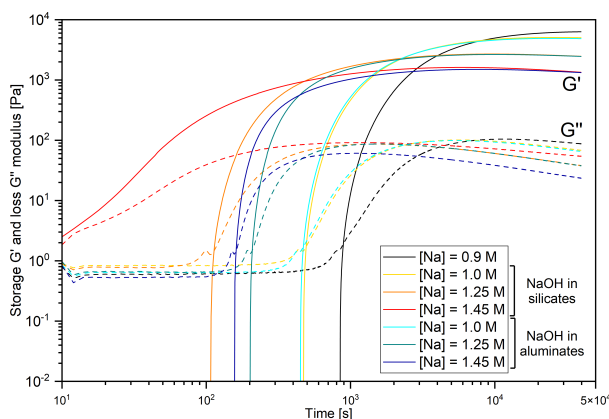

Fig. S3: Kinetics of gelation if an excess of NaOH is introduced either in the silicate solution or in the aluminate solution. [Si] = 1.125 mol·L^{-1}, [Al] = 0.12 mol·L^{-1}

3 Homogeneous vs inhomogeneous gels

As discussed in the main text, the homogeneity of the gels produced varies with the composition as reported in the ternary phase diagram (Fig.1). Here we show images of a homogeneous gel and an inhomogeneous gel, which appears lumpy.
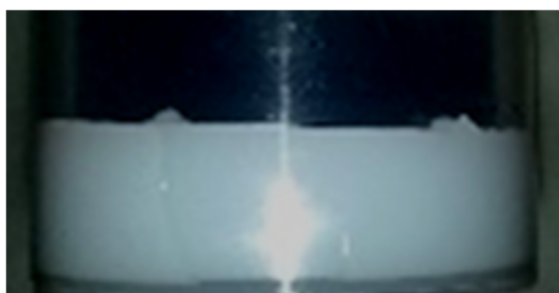
Homogeneous gel

Inhomogeneous gel

Fig. S4: Photos of homogeneous gel (solid red zone of ternary phase diagram shown in Fig.1) and inhomogeneous gel (red hatched zone of ternary diagrams in Fig.1)

4 Effect of the temperature on the viscoelastic modulus

The kinetics of gelation are faster when the temperature increases, but the values of G' and G'' that develop in the mature gel seem independent of the temperature, as reported in Figure S5 A. From these experiments and for various chemical formulations, we were able to calculate the activation energy from an Arrhenius plot (Figure S5 B). The value of the flow activation energy Ea is found to be independent of the chemical formulation and has a value of 60 kJ·mol^{-1}.

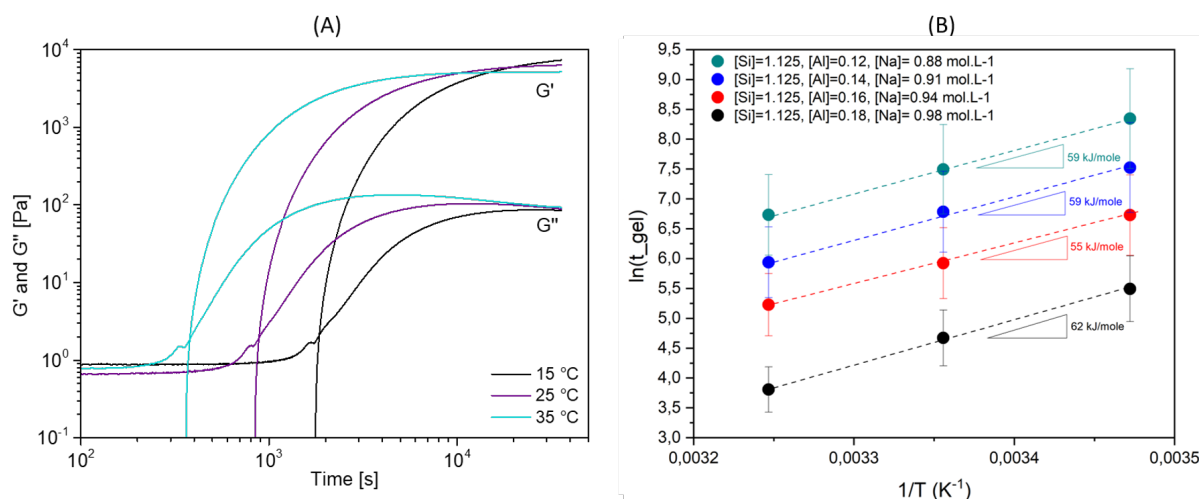Fig. S5: (A) Effects of temperature on the kinetics of gelation for the $[Si] = 1.125$ mol·L^{-1}, $[Al] = 0.12$ mol·L^{-1}, $[Na]$ = 1.31 mol·L^{-1} formulation, (B) Determination of activation energy for four chemical formulations; vary from 59 to 75 kJ·mol^{-1}

5   Fractional Maxwell Gel Model (FMG) parameters

The influence of the aluminum concentration (by keeping the concentration of Si and Na fixed) on the FMG parameters is shown in Figure S6. at a reference concentration of $[Al] = 0.106$ mol·L^{-1}, the values are $\mathbb{V}_1 = 7020$ Pa.s$^{\alpha}$, $\mathbb{G}_1 = 643$ Pa, $\alpha_1 = 0.39$ and $\tau_1 = (\mathbb{V}_1/\mathbb{G}_1)^{1/\alpha_1} = 483$ s. As the $[Al]$ concentration is increased both $\mathbb{V}$ and $\mathbb{G}$ increase; however, the power law exponent (which is related to the fractional dimension of the critical gel formed at the time t_{gel}) remains invariant.
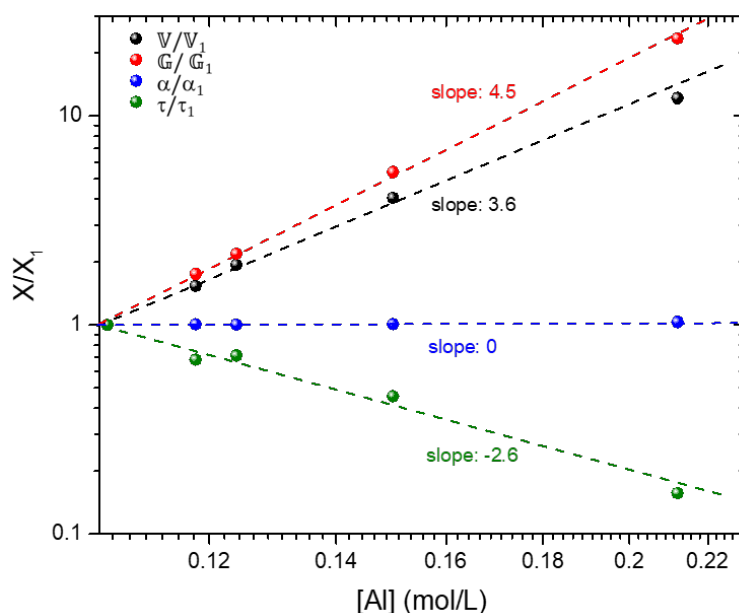

Fig. S6: τ/τ_1, α/α_1, $\mathbb{V}/\mathbb{V}_1$ and $\mathbb{G}/\mathbb{G}_1$ determined from fitting the experimental frequency sweep data in Fig. 4 with the FMG model.

6   Scaling for other chemical compositions: stoechiometrically unbalanced formulations

As we discuss in the main text (and our previous work, Keshavarz *et al.* (2021) the composition of the gels can be varied by modifying the aluminum and the sodium concentrations at the same time. Dimensionless master curve for five chemical formulations (corresponding to stoechiometrically unbalanced samples) is presented in Figure S7. We construct a master

Table S1: Fitting parameters obtained from FMG model for various chemical compositions.

[Al] (mol·L^{-1})	$\mathbb{V}$ (Pa.s$^\alpha$)	$\mathbb{G}$ (Pa)	α	τ (s)
0.106	7020	643	0.39	483
0.118	10791	1128	0.39	329
0.124	13625	1406	0.39	344
0.150	31473	3461	0.39	287
0.212	85399	15079	0.4	76

curve for this data in the same manner as described for the stoechiometrically balanced formulations discussed in the main text. The horizontal shift is performed by using a relaxation time calculated from the fractional gel model and the vertical shift consists of normalizing by the elastic plateau G_0.
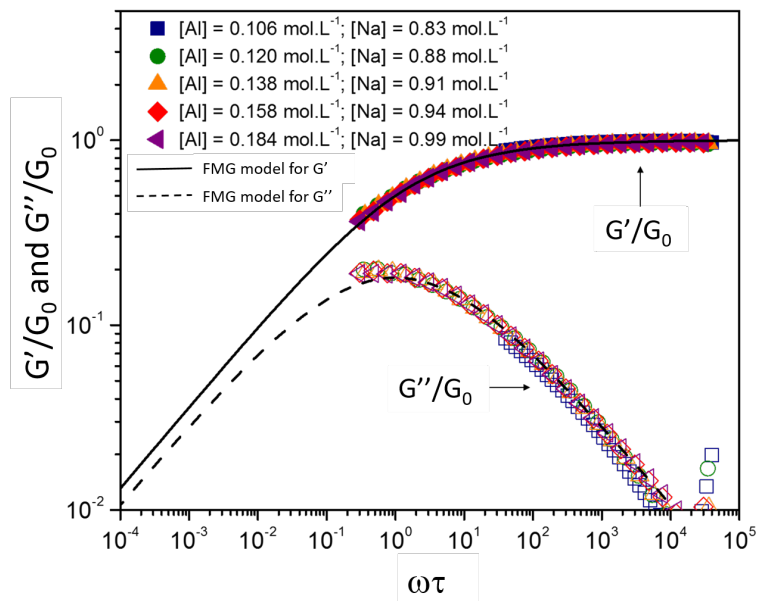

Fig. S7: Dimensionless master curve for five chemical formulations (unbalanced samples). Dimensionless values of viscoelastic moduli G'/G_0 and G''/G_0 are plotted as a function of the reduced frequency $\omega\tau$. Solid and dashed lines show the dimensionless predictions of the FMG model using the parameter values in Table S1

.

7 Strain sweep on the unbalanced formulations

The strain sweep for the set of unbalanced formulations is presented in Figure S8. The limit of linearity decreases when the aluminum content increases and this latter parameters roughly representing the volume fraction of particles.
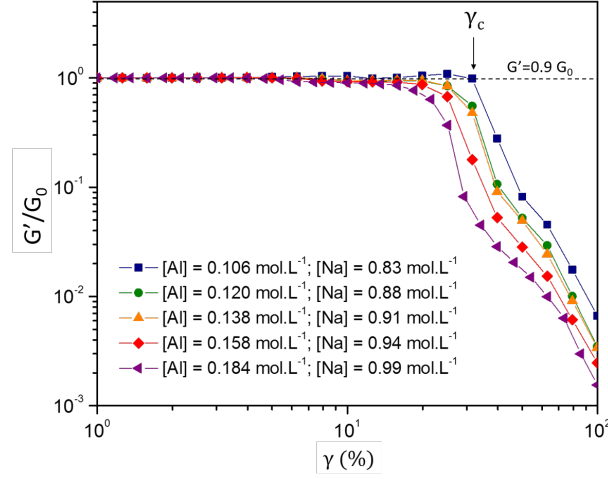
Fig. S8: Experimental G' normalized by the plateau modulus, G_0, as a function of the strain amplitude γ, for various unbalanced formulations with [Si] = 1.125 mol·L^{-1}. Here γ_c represents the critical strain when G' = $0.9G_0$.

8 Fractional Maxwell Gel model parameters for the unbalanced formulations

For the set of unbalanced formulations, the influence of the aluminum concentration on the FGM parameters is presented in Figure S9. $\mathbb{V}_1$=54724 Pa.s$^\alpha$, $\mathbb{G}_1$=3186 Pa, α_1=0.45, τ_1=400 s
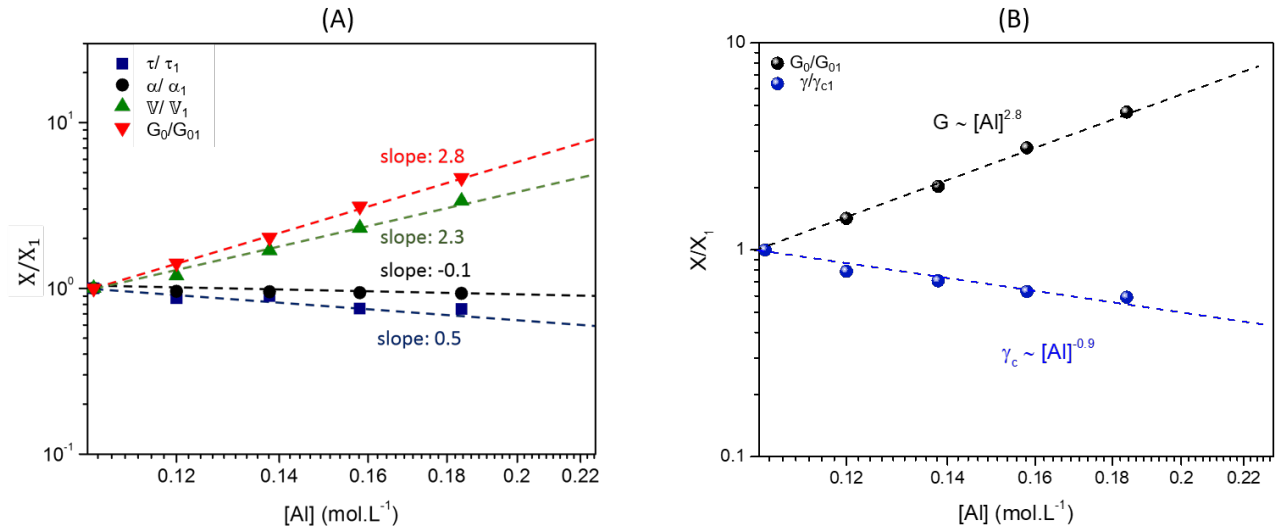

Fig. S9: Variation in the ratios τ/τ_1, α/α_1, $\mathbb{V}/\mathbb{V}_1$ and G_0/G_{01} determined from fitting the FMG model to the data in Figure S7 and Table S2 for unbalanced formulations.

Table S2: Fitting parameters obtained from FMG model for stoechiometrically balanced formulations.

[Al] (mol·L^{-1})	[Na] (mol·L^{-1})	$\mathbb{V}$ (Pa.s$^\alpha$)	$\mathbb{G}$ (Pa)	α	τ (s)
0.106	0.83	54724	3186	0.47	400
0.120	0.88	65079	4524	0.45	348
0.138	0.91	92495	6453	0.45	358
0.158	0.94	126390	9925	0.45	302
0.184	0.99	183740	14774	0.44	301

In Figure S9-A we observe that the aluminum concentration dependence for the unbalanced gel formulations are weaker than those for the stoechiometrically balanced formulations (Fig. S6). By combing the results from Figures S9-A and S8, we obtain the evolution of the elasticity and the critical strain as a function of aluminum concentration. (Fig. S9-B) with power law exponents $\mu = 2.8$ and $\nu = 0.9$. These exponents are lower than for the other set of chemical formulation suggesting a modification of the strength balance between intra- floc interactions and inter-floc interactions i.e.

the backbone links within the clusters seems to become stronger and their stiffness grows to a level comparable to the inter-cluster links. However, the situation is further complicated because both Al and Na concentrations vary concomitantly with an antagonist effect. The aluminum ions act as bond makers whereas sodium ions act as bond breakers. Indeed, in Fig. S12, we show a decrease of the viscoelastic modulus (the power law exponent is close to 5.1) as a function of the sodium concentration, even with a constant concentration of aluminum. It is thus possible that sodium ions come around the building blocks and the clusters to compensate the negative charges of the aluminosilicate species, limiting their interactions. Scattering data support this assumption because the average size of clusters and building blocks is larger for the highest sodium concentration with as an identical fractal dimension (d_f = 2.1), see Table S3 .

9 Influence of NaOH on the mechanical spectra and on the fractional parameters

The influence of the NaOH concentration on the linear viscoelastic properties is presented in Figure S10. Increasing the alkalinity of the solution produces a weaker gel. Once agmain the upturn in $G"(\omega)$ at very high frequency is an indicator of rotational inertia in the rheometer fixture and this data is not included in the fitting. The fractional parameters as a function of the sodium concentration are plotted in Figure S11. Unlike the other formulations, $\mathbb{V}$ and G_0 decrease, and the exponent α slightly decreases, signifying an increase of the relaxation time with higher sodium concentrations. This later result suggests that the size of the clusters is bigger, which is consistent with the USAXS data presented in the main text. Here, $\mathbb{V}_1$=10791 Pa.s$^\alpha$, G_{01}=1128 Pa, α_1=0.39, τ_1=329 s.
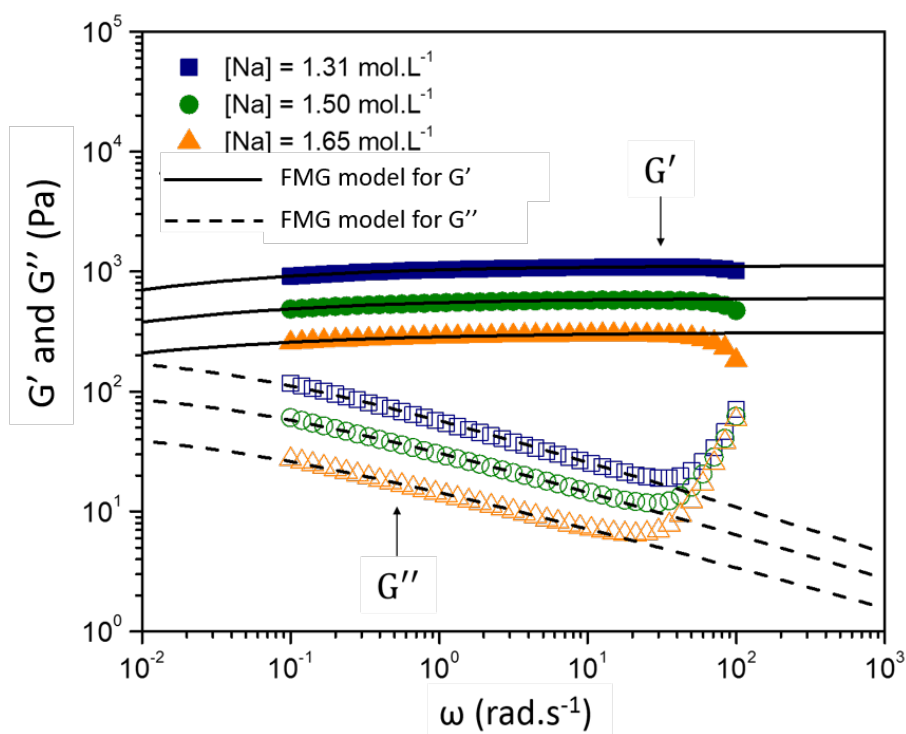

Fig. S10: Viscoelastic moduli as a function of frequency, for various sodium concentrations with [Si] = 1.125 mol·L^{-1} and [Al] = 0.118 mol·L^{-1}. Fractional Maxwell Gel Models are used to describe the experimental data.
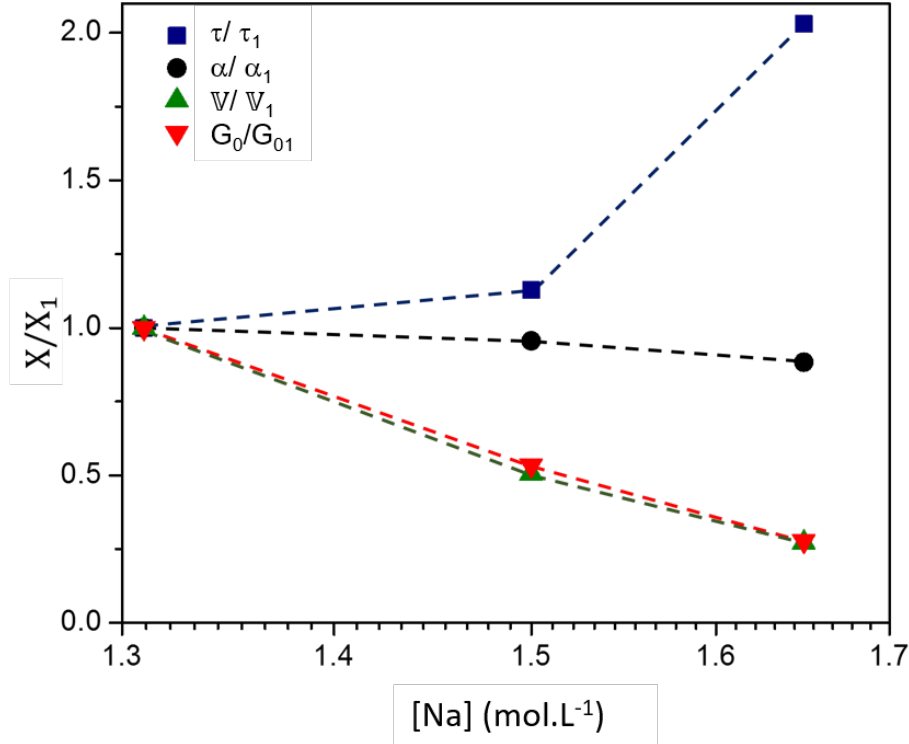
Fig. S11: Influence of sodium concentration on the FMG model parameters: τ/τ_1, α/α_1, $\mathbb{V}/\mathbb{V}_1$ and G_0/G_{01},

10   USAXS data treatment

The scattering intensity over the whole q-range (USAXS data in Figure 7) is modeled by Eq. SI-1, Keshavarz *et al.* (2021). The first term is a Porod law describing the surface scattering of a superstructure. The second term uses a Guinier-Porod model (Hammouda (2010)) that interpolates between a Guinier regime at low q and a power-law Porod scaling at large q. The crossover between the two regimes is controlled by a characteristic length scale R_g. In order to account for successive structural levels covering different ranges of length scales, two structural levels in the intermediate q range were used. A structure factor $S(q)$ is also used in this model to take into account the correlation between entities inside the clusters. The third term is also a Guinier-Porod model used to describe the small silicate entities remaining in the solution that do not participate to the gel scattering.

$$I(q) = \left[\frac{G_2}{q^{s_2}} \exp\left(-\frac{q^2 R_{g,2}^2}{3 - s_2} \right) + \frac{G_1}{q^{d_f}} \exp\left(-\frac{q^2 R_{g,1}^2}{3 - d_f} \right) + \frac{B}{q^{d_1}} \right] S(q) + \frac{G_0}{q^{s_0}} \exp\left(-\frac{q^2 R_{g,0}^2}{3 - s_0} \right) + \frac{C}{q^{d_0}} \qquad (1)$$

where

$$G_2 = G_1 \exp\left[-q_2^2 \left(\frac{R_{g,1}^2}{3 - d_f} - \frac{R_{g,2}^2}{3 - s_2} \right) \right] q_2^{(s_2 - d_f)}, \quad B = G_1 \exp\left(-\frac{q_1^2 R_{g,1}^2}{3 - d_f} \right) q_1^{(d_1 - d_f)}, \quad C = G_0 \exp\left(-\frac{q_0^2 R_{g,0}^2}{3 - s_0} \right) q_0^{(d_0 - s_0)}$$

$$(2)$$

and

$$q_2 = (d_f - s_2)^{1/2} \left[\frac{2 R_{g,2}^2}{3 - s_2} - \frac{2 R_{g,1}^2}{3 - d_f} \right]^{-1/2}, \quad q_1 = \frac{1}{R_{g,1}} \left[\frac{(d_1 - d_f)(3 - d_f)}{2} \right]^{1/2}, \quad q_0 = \frac{1}{R_{g,0}} \left[\frac{(d_0 - s_0)(3 - s_0)}{2} \right]^{1/2}$$

$$(3)$$

where q_i represent the transition regions for describing each level of scattering with $q_2 \leq q_1 \leq q_0$. From the point of view of the characteristic length-scales, this means that $R_{g,2} \geq R_{g,1} \geq R_{g,0}$. B and C are the Porod constants and G_1, G_0 are fitting constants. The values of s_0, s_2 and d_f represent the structural parameters used to model non spherical objects. d_f is specifically related to the fractal dimension of the clusters. Values of $R_{g,i}$ with $i = 0, 1$ and 2 are the radii of gyration and d_0 and d_1 represent the Porod exponent for level 0 and 1 respectively.

An empirical structure factor was used to take into account the appearance of some correlated regions after the critical point (sol/gel transition). The expression for $S(q)$ is given by:

$$S(q) = 1 + C_0 \left[\left(\frac{q}{q_0} \right)^2 + \left(\frac{q}{q_0} \right)^{-2} \right]^{-1} \tag{4}$$

where C_0 is a constant and q_0 is the position of the maximum of the correlation peak. This expression leads to the following asymptotic limits:

$$\lim_{q \to \infty} S(q) = 1, \quad \lim_{q \to 0} S(q) = 1 \quad \text{and} \quad S(q) = 1 + \frac{C_0}{2} \quad \text{for} \quad q = q_0$$

The measured USAXS data are fitted with the scattering model (1) and the fitting parameters for the chemical compositions presented in Figure 7 are tabulated in Table S2.

Table S3: Fitting parameters of the scattering model fitted to the USAXS data of various chemical compositions.

Aluminosilicate gels	G_1	G_0	$R_{g,2}$ (Å)	$R_{g,1}$ (Å)	$R_{g,0}$ (Å)	s_2	d_f	s_0	d_1	d_0	C_0	q_0
1. $Si_{1.125}\text{-}Al_{0.12}\text{-}Na_{1.65}$	0.02	0.17	2772	24.2	3.95	0.5	2.1	0.0	4.0	2.0	0.6	0.02
2. $Si_{1.125}\text{-}Al_{0.106}\text{-}Na_{0.83}$	0.028	0.16	685	17.7	4.3	0.2	2.0	0.0	4.0	2.0	2.0	0.04
3. $Si_{1.125}\text{-}Al_{0.106}\text{-}Na_{1.31}$	0.0155	0.15	1700	18.1	3.85	0.4	2.1	0.0	4.0	2.45	1.3	0.023

11 Influence of the chemistry on the elasticity at equilibrium

The influence of varying the concentration of each chemical element, while keeping the two other components constant, on the plateau elastic modulus in the fully-developed gel is presented in Figure S12. We observe a power law dependency of the elastic modulus of the gel, with a negative exponent for the effect of Na, and a positive exponent for both Al and Si.
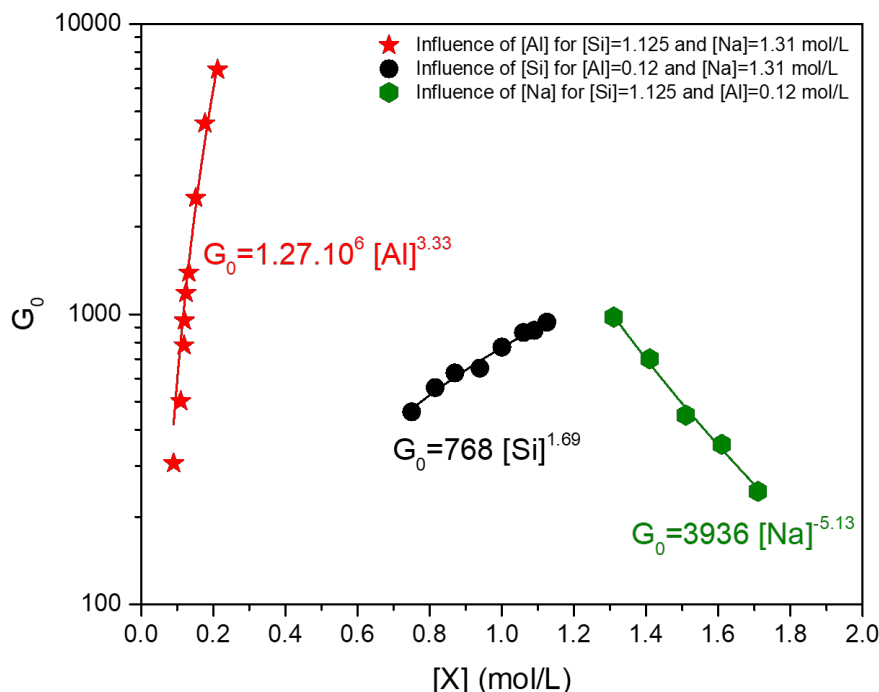

Fig. S12: Evolution of the plateau elastic modulus at equilibrium, for varying concentration of each chemical component in the aluminosilicate gels while keeping the two other constant. X correspond to either Al, Si or Na

12   Evolution of the gel volume over time

The evolution of the volume of the gel (normalized by its initial value) as a function of time is presented in Figure S13. The destabilization and collapse of the gel seems to be postponed when the sodium concentration is low.
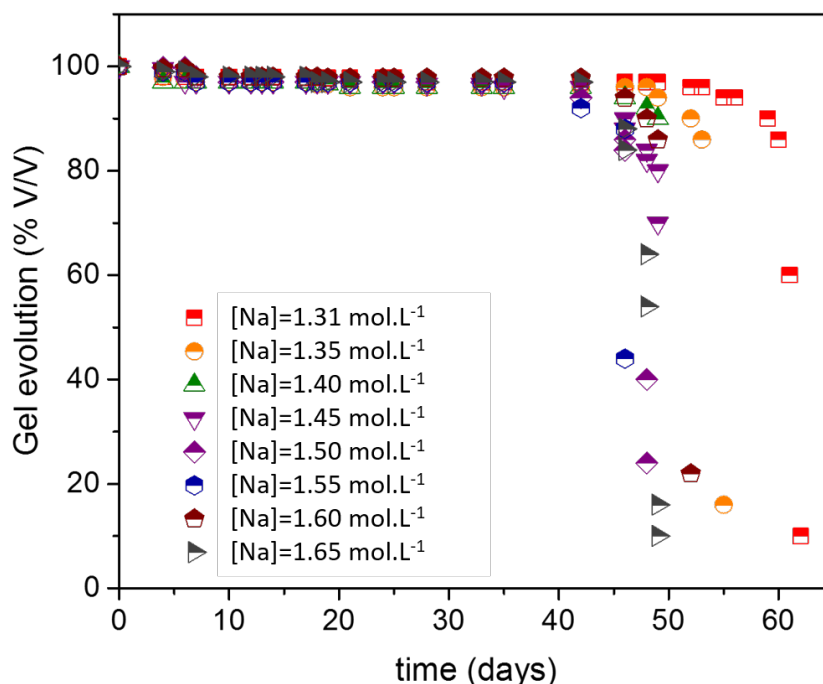

Fig. S13: Evolution in the Volume occupied by the gel during the early aging at 40 °C, for gels formulated with various sodium concentrations in [Si] = 1.125 mol·L^{-1} and [Al] = 0.118 mol·L^{-1}

13   X-Ray Diffraction patterns of the zeolites synthesized at 40 and 50 °C

The influence of the initial concentration of aluminum and sodium on the XRD patterns for samples synthesized at 40 and 50 °C is presented in Figures S14, S15, and S16. For the synthesis carried out at 40 °C, it is observed that whatever the initial concentration of aluminum and sodium, the main crystalline precipitate is Chabazite. At 50 °C, additionnal peak of Gmelinite (presenting exactly the same stoechiometry of chabazite but that do not crystallize in the same form) is observed around $2\theta = 27$ degrees. The XRD patterns do not seem modified by the increase of the aluminum concentration, whereas an increase of the initial sodium amount results in the narrowing of the peaks centered around $2\theta \sim 9, 21, 53°$ (Figures S14 and S15). The peak narrowing is related to an increase of the crystalline domain size (Holder and Schaak (2019)), that is also consistent with the USAXS results presented in the main text. At 50 °C, the transformation of the zeolite particles ($20 < 2\theta < 24°$) into Chabazite type is noticed. In Figure S17, we compare specifically the influence of the aging temperature for two concentrations of aluminum ions. The diffraction peaks are narrower at 40 °C meaning the size of crystallites are larger. This is certainly due to the fact that at low temperature the zeolites have more time to nucleate and growth (zeolites precipitate in 60 days at 40 °C as compared to 30 days at 50 °C).
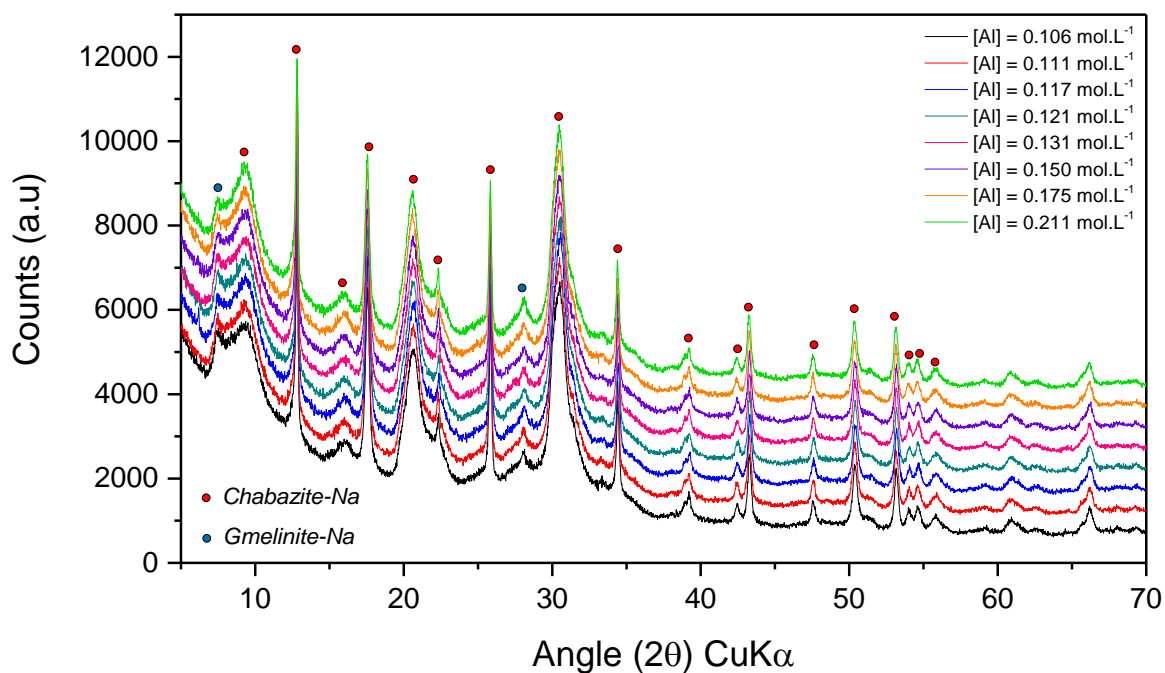
Fig. S14: Influence of aluminum concentration on the XRD patterns of aluminosilicate crytals obtained after aging at 40 °C. [Si] = 1.125 mol·L^{-1} and [Na] = 1.31 mol·L^{-1}
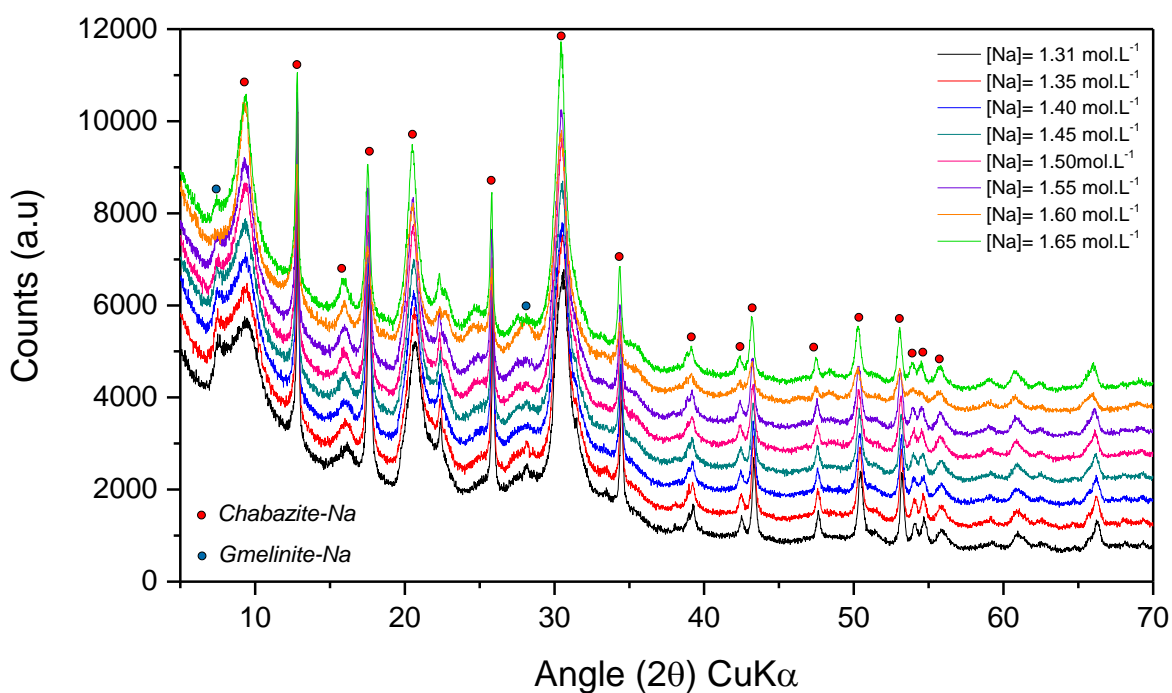

Fig. S15: Influence of sodium concentration on the XRD patterns of aluminosilicate crytals obtained after aging at 40 °C. [Si] = 1.125 mol·L^{-1} and [Al] = 0.12 mol·L^{-1}
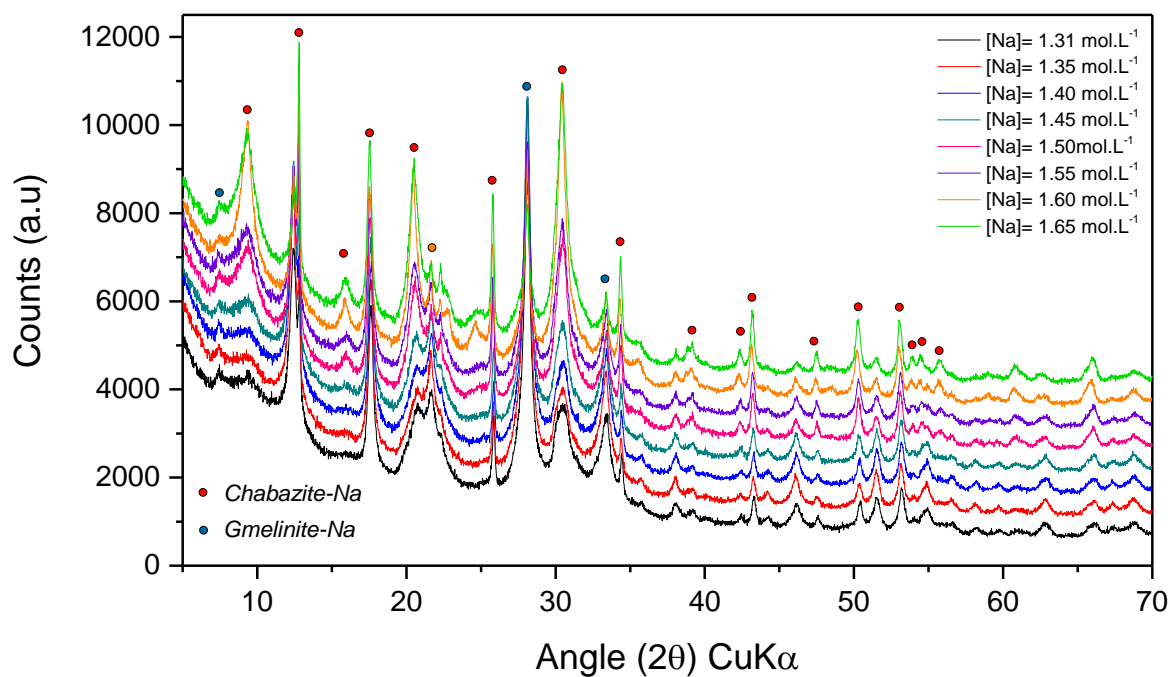
Fig. S16: Influence of sodium concentration on the XRD patterns of aluminosilicate crytals obtained after aging at 50 °C. [Si] = 1.125 mol·L^{-1} and [Al] = 0.12 mol·L^{-1}
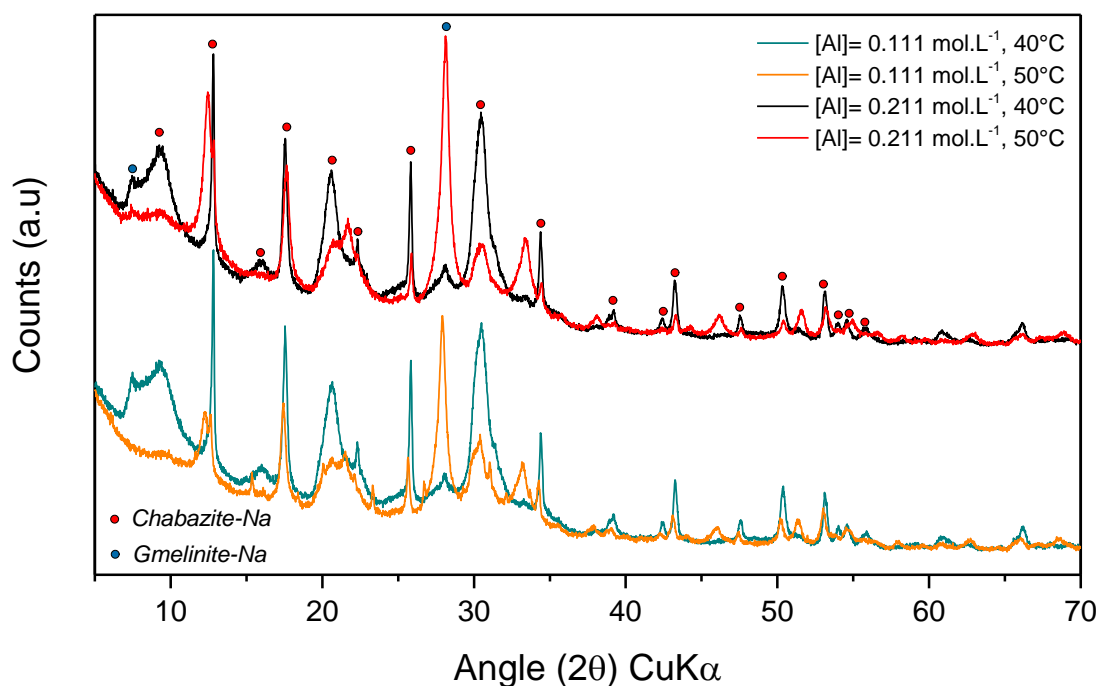

Fig. S17: Influence of the gelation and curing temperature on the diffraction patterns for two concentrations of aluminum. [Si] = 1.125 mol·L^{-1} and [Na] = 1.31 mol·L^{-1}

References

B. Keshavarz, D. G. Rodrigues, J.-B. Champenois, M. G. Frith, J. Ilavsky, M. Geri, T. Divoux, G. H. McKinley and A. Poulesquen, *Proceedings of the National Academy of Sciences*, 2021, **118**, e2022339118.

B. Hammouda, *Journal of Applied Crystallography*, 2010, **43**, 716–719.

C. F. Holder and R. E. Schaak, *ACS Nano*, 2019, **13**, 7359–7365.